Quantification of toxic metallic elements using machine learning techniques and spark emission spectroscopy

Seyyed Ali Davari[1,2,*] and Anthony S. Wexler[1,2]

[1]Air Quality Research Center (AQRC), University of California, Davis, 95616, Davis, USA
[2]Department of Mechanical and Aerospace Engineering, Civil and Environmental Engineering, and Land, Air and Water Resources, University of California, Davis, USA

Abstract

The United States Environmental Protection Agency (US EPA) list of Hazardous Air Pollutants (HAPs) includes metal elements suspected or associated with development of cancer. Traditional techniques for detecting and quantifying toxic metallic elements in the atmosphere are either not real time, hindering identification of sources, or limited by instrument costs. Spark emission spectroscopy is a promising and cost effective technique that can be used for analyzing toxic metallic elements in real time. Here, we have developed a cost-effective spark emission spectroscopy system to quantify the concentration of toxic metallic elements targeted by US EPA. Specifically, Cr, Cu, Ni, and Pb solutions were diluted and deposited on the ground electrode of the spark emission system. Least Absolute Shrinkage and Selection Operator (LASSO) was optimized and employed to detect useful features from the spark-generated plasma emissions. The optimized model was able to detect atomic emission lines along with other features to build a regression model that predicts the concentration of toxic metallic elements from the observed spectra. The limits of detections (LOD) were estimated using the detected features and compared to the traditional single-feature approach. LASSO is capable of detecting highly sensitive features in the input spectrum; however for some elements the single-feature LOD marginally outperforms LASSO LOD. The combination of low cost instruments with advanced machine learning techniques for data analysis could pave the path forward for data driven solutions to costly measurements.

1 Introduction

The United States Environmental Protection Agency (US EPA) lists a number of metals in their list of Hazardous Air Pollutants (HAPs). These metals are known or suspected to cause cancer or other serious health effect Buzea et al. (2007); Pope III et al. (2002). Table 1 lists the metals in US EPA's HAPs list. Table 2 lists other metals that are not on US EPA's HAPs list but have been implicated in a range of

Table 1: List of hazardous metallic elements targeted by US EPA

US EPA Metal HAPS
Antimony
Arsenic
Beryllium
Cadmium
Chromium
Cobalt
Lead
Manganese
Mercury
Nickel
Selenium

Table 2: List of other toxic metals

Metallic Element
Copper
Iron
Zinc

adverse health effects so are of concern to the California Air Resources Board (CARB). It has been shown that presence of these metals are associated with various health concerns such as diabetes (Zanobetti et al. (2009)), cardiovascular disease (Brook et al. (2004)), and asthma (Gent et al. (2009)). Therefore, it is necessary to monitor and quantify their ambient concentration.

Various techniques over the years have been developed and used to measure metal particles. X-ray fluorescence (XRF) Van Meel et al. (2007); Vincze et al. (2002) and inductively coupled plasma mass spectrometry (ICP-MS) Rovelli et al. (2018); Venecek et al. (2016) have been used traditionally to quantify metals in atmospheric particles. XRF is excellent for measuring lighter elements and metals on filter substrates, but for field application it is expensive, has a high limit of detection (LOD) for heavier elements, and includes radiation risk. ICP-MS requires collection of aerosol on a substrate, such as a filter or impactor foil, extraction of the metals or elements from the substrate using harsh acidic chemicals, and then analyzing in the ICP-MS along with standards that help the instrument quantitate. Moreover, ICP-MS is most suitable for heavier elements and metals so has a high LOD for lighter toxic metals and is not available in field-deployed, real-time applications. Additionally, these instruments are expensive and hence are limited by cost and complexity as well.

Spark-induced breakdown spectroscopy (SIBS) and laser-induced breakdown spectroscopy (LIBS) have been employed in various applications from combustion Do and Carter (2013); Kiefer et al. (2012); Kotzagianni et al. (2016), nanomaterials Davari et al. (2017a); De Giacomo et al. (2011); Hu et al. (2017); Matsumoto et al. (2015a,b, 2016), and environmental/bio-hazards Diwakar et al. (2012); Diwakar and Kulkarni (2012); Zheng et al. (2018), forensics Martin et al. (2007), semiconductors and thin films Axente et al. (2014); Davari et al. (2017b, 2019); Hermann et al. (2019), explosives Gottfried et al. (2009), pharmaceuticals Mukherjee and Cheng (2008a,b); St-Onge et al. (2002), and biomedical Abbasi et al. (2018); Baudelet et al. (2006); Davari et al. (2018). Particularly, Fisher et al. (2001) studied various toxic metals in aerosols by optimizing the spectrometer response with respect to gate delay. Hunter et al. (2000) employed spark

emission spectroscopy for continuous monitoring of metallic elements in aerosols. Yao et al. (2018) used spark emission spectroscopy to obtain the carbon content of fly ashes. Diwakar and Kulkarni (2012) employed spark emission spectroscopy coupled with a corona aerosol microconcentrator (CAM) to improve the particle collection efficiency and detection limits of toxic metallic elements. Zheng et al. (2017) characterized the CAM performance with respect to different experimental parameters and obtained the optimized design parameters for their CAM system.

While LIBS and SIBS address issues regarding the field measurement and instrument complexity, they are still considered expensive. Current interest in low-cost sensors and their ability to characterize local air pollution concentrations motivated development of a low-cost system. We employed two complementary approaches: (1) decreasing the cost of the electronics associated with SIBS and (2) incorporating advanced data analysis techniques to improve quantification and limit of detection. In recent years, numerous studies have used artificial neural networks (Ferreira et al. (2008)), partial least square and least absolute shrinkage and selection operator (LASSO) (Dyar et al. (2012)) on emission spectra to improve the quantification and limit of detection of spectroscopic systems. In this study, we have developed a low-cost spark emission spectroscopy system to quantify toxic metallic elements. The expensive components such as spark generation and delay generator have been developed to reduce the overall cost. To improve performance, advanced machine learning tools such as K-Means clustering and LASSO have been employed to improve the system performance. The resulting instrument was evaluated against four toxic metallic elements listed by US EPA.

2 Instrument development:

2.1 Spark generation system:

One costly component that is required for developing a spark emission spectroscopy system is the spark generation system. Numerous papers have studied the fundamental principles of spark emission spectroscopy Sacks and Walters (1970); Walters (1969, 1977). The key idea is to discharge a capacitor as quickly as possible to increase the power dissipated in the spark gap. Fig. 1 illustrates the schematic of the spark generation system. The overall goal is to charge a capacitor at high voltage and once it has been charged sufficiently,

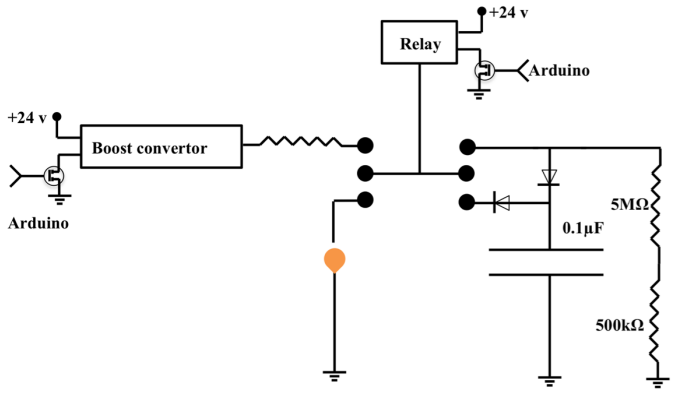

Figure 1: Schematic of the built-in spark generation system.

discharge the capacitor through the spark gap. An Arduino board controls the timing between charging and discharging the capacitor. A boost convertor converts 24v DC to 5000v DC and is connected to a mechanical relay with two switching states controlled with the Arduino board. In the charge state, the mechanical relay provides the conduction path between the boost convertor and the capacitor. In this configuration, the capacitor reaches full charge in 5μs. Once the capacitor is fully charged, the Arduino board sends a signal to turn off the boost convertor and sends another signal to the mechanical relay to flip to the discharge state. At the discharge state, the mechanical relay provides a conduction path between the capacitor and the spark gap. Previous studies by Shepherd et al. (2000) showed that the discharge process could be controlled by a resistor after the spark gap. For low resistor values, the spark current exhibited a periodic behavior as the capacitor discharges, which can be associated with an under damped discharging. On the other hand, increasing the resistor value damped the discharge process and dissipated a large portion of the capacitor

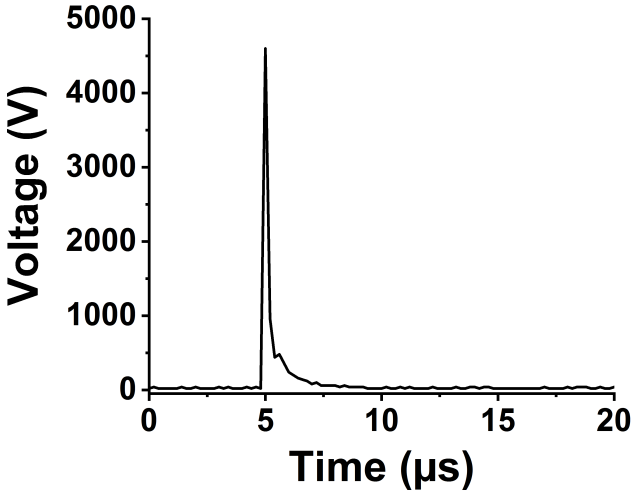

Figure 2: Spark voltage evolution in time.

energy through the resistor instead of the spark gap.In our setup, a 10Ω resistor maximizing power dissipation in the spark gap, while minimizing oscillations. Fig. 2 illustrates the evolution of the generated spark as a function of time. The voltage shows a sudden increase followed by an exponential decrease fully discharging in less than 5μs and thus delivering sufficient energy to the arc and deposited analyte.

2.2 Delay generator:

The delay generator is another costly component typically used in time-resolved spectroscopy. Electronics advances have paved the way for developing a cost-effective delay generator. The delay generator suppresses initial noise in the emission spectrum so needs to cover a range between 1μs and 20μs with resolution less than 0.2μs. We designed a custom-built delay generator in order to lower the overall cost of the instrument. Fig. 3

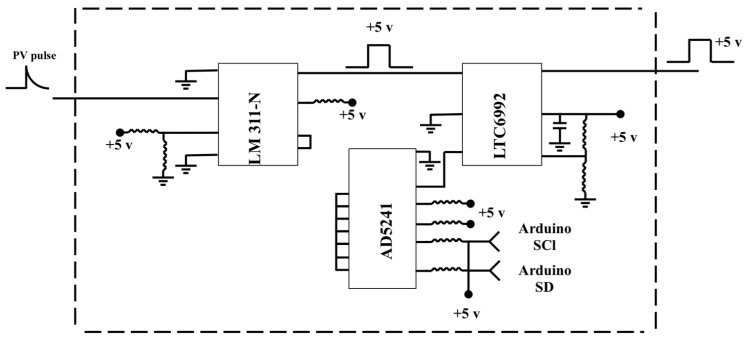

Figure 3: Schematic of the built-in delay generator.

illustrates the schematic of the circuit. Upon generation of the spark-induced plasma, a pair of lenses collects and focuses the plasma emission into a photodiode. The pulse generated by the photodiode is passed into a voltage comparator (LM 311-N) to generate a transistor–transistor logic (TTL) signal. The output TTL signal from the comparator is sent to a pulse width modulator (PWM) controller (LTC6992), which adds delay to the TTL signal. An Arduino board adjusts a digital resistor (AD5241), which in turn determines the delay value. Fig. 4 shows the delay generator performance. The Y axis illustrates the delay values requested of the delay generator while the X axis shows the measured values. The red dashed line shows the desired 1:1 line while the circles show the measured performance. The performance is linear over with a slight deviation from the 1:1 line. Considering the spark generated plasma short lifetime, our measurements require short delay values ($< 5\mu$s) where the built-in delay generator shows excellent performance and accuracy.

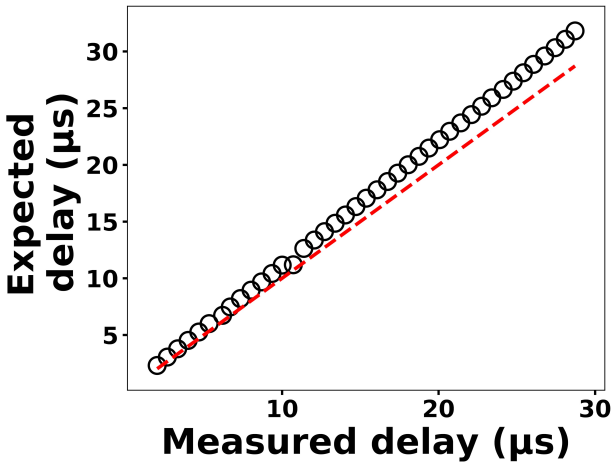

Figure 4: The expected delay set by the Arduino board as a function of the measured delay.

2.3 Spectra Collection:

Four toxic metallic elements with different concentrations were used to test the developed spark emission spectrometer system performance. Cr, Cu, Ni and Pd (1000μg/mL) were purchased from AccuStandard and diluted to specific concentrations. A micropipette was used to deposit diluted solutions on a 1 mm diameter Tungsten ground electrode of the spark system for emission analysis. The total mass can be calculated from the deposited volume and solution concentration. Upon evaporation of the droplets, the capacitor was discharged to ablate the deposited material and obtain spectra. A pair of lenses (75mm focal length and 1" diameter, Thorlab) focused the emission into an optical fiber connected to a spectrometer (Ocean Optics).

3 Results and discussions:

To address shot-to-shot variations in the spark-generated plasma and nullify possible faults caused by the low cost components, an unsupervised learning technique, K-Means clustering, classifies the collected spectra. Following this procedure, it is possible to identify and remove outliers and hence improve the accuracy of

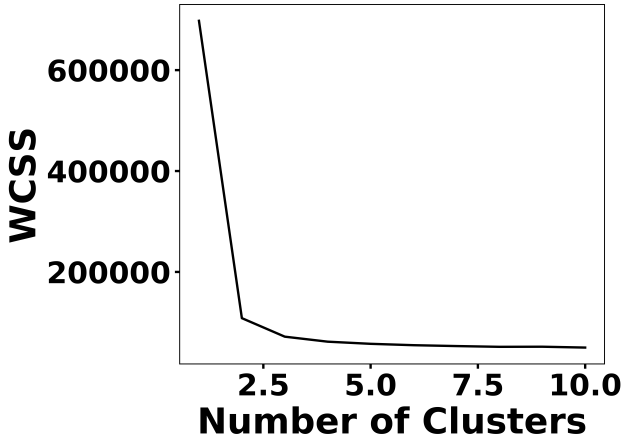

Figure 5: The elbow plot suggests two centroids for clustering the spectra set.

the analysis. Fig. 5 illustrates the elbow plot that is used to optimize the number of spectral classes. The standard approach is to set the optimum number of clusters to the value where the within-cluster sum of squares (WCSS) error plateaus. The WCSS error plateaus once we have two or more centroids and

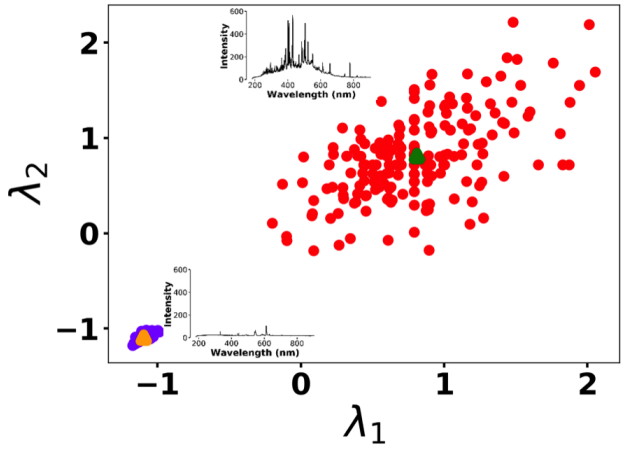

Figure 6: K-Means clustering for detecting outliers before passing the spectra set to LASSO model. Two clusters were plotted for the normalized intensities of two arbitrary wavelengths at λ_1 (208.365 nm) and λ_2g (208.759 nm).

therefore, the number of centroids is set to two. Fig. 6 illustrates the performance of the model for 300 spectra obtained from the background (Tungsten ground electrode ablation). The results show clearly two clusters with different emission response. The lower left cluster containing $< 10\%$ of the spectra represent low-signal outliers so were eliminated from further analysis. For each element, 0.1, 1, 10 and 100 ng of mass were deposited on the ground electrode. For each concentration, 10 spectra were collected using 2 μs delay between the observed and recorded emissions. Feature scaling is a standard preprocessing step that improves the model optimization process. A series of Tungsten lines were used to estimate the plasma temperature for the recorded cleaned spectra set at 2μs . Fig. 7 illustrates the Boltzmann plot constructed by Tungsten lines. Based on the slope of the fit, the plasma temperature is estimated as 4013 $\pm$ 579 K. Upon

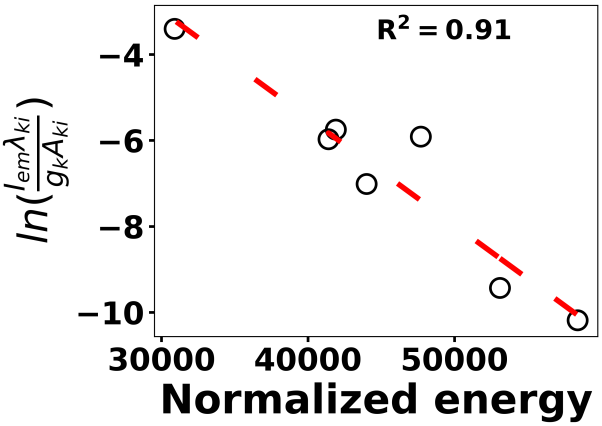

Figure 7: Boltzmann plot for various Tungsten lines in order to estimate plasma temperature.

identifying and removing the outlier spectra, the cleaned spectra set is normalized using the Tungsten peak at W I (400.87 nm) and fed into the Least Absolute Shrinkage and Selection Operator (LASSO) algorithm for model development and prediction.

LASSO:

The cleaned scaled spectra set has been used to detect and quantify concentrations of the toxic metals. Simple linear regression obtains the slope and intercept of a linear line by minimizing the mean squared

error between the predictions and known values. Least absolute shrinkage and selection operator (LASSO) detects and employs more features to perform predictions by optimizing the following loss function:

$$J(\boldsymbol{\theta}) = \frac{1}{m}\sum_{i=1}^{m}(y^{(i)} - h_\theta(\mathbf{x}^{(i)}))^2 \; + c\sum_{j=1}^{k}|\theta_j| \tag{1}$$

where $\mathbf{x}^{(i)} \in \mathbb{R}^{2048}$ and $h_\theta(\mathbf{x}^{(i)})$ represent the normalized spectrum and the LASSO concentration prediction based on spectrum (i) ($\mathbf{x}^{(i)}$), respectively, where $y^{(i)}$ is the known concentration corresponding to spectrum (i). The LASSO coefficients are indicated by θ_j. The first term in equation (1) is the mean squared error and is common with simple linear regression, while the second term is a regularization term that minimizes the magnitude of θ_j. The L1 norm essentially sets most of the features in the spectrum to zero and maintains only

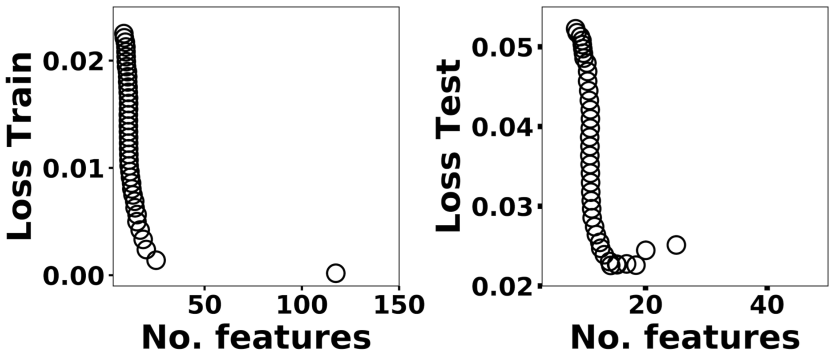

Figure 8: The train and test losses for Ni as a function of number of features.

a few features to build the linear model and perform predictions. The regularization constant (c) determines the number of features to be used in the model, and therefore the model loss needs to be optimized with respect to the regularization constant. To obtain the optimized regularization constant, we plotted the loss values for the Ni spectra training and testing sets as a function of number of features for various c values based on Leave-One-Out cross validation (Fig. 8). As expected, the train loss monotonically decreases as the number of features increases, while the loss for the test set initially decreases and then starts increasing. This implies that after incorporating a certain number of features into the model, the model starts memorizing

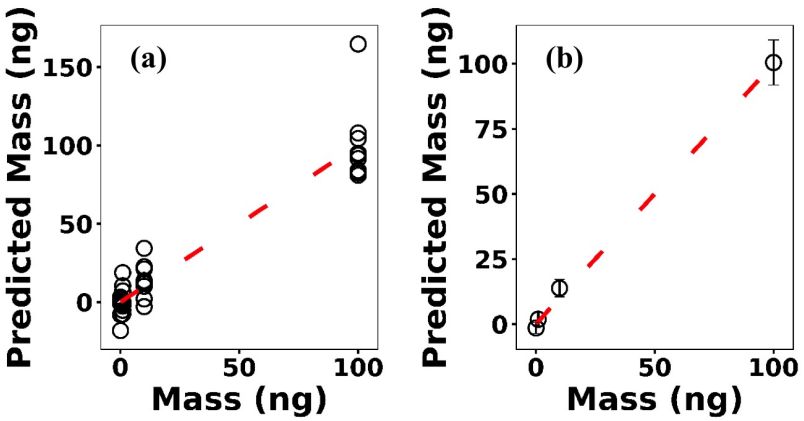

Figure 9: (a) LASSO predictions based on Leave-One-Out cross validation for Ni , (b) the averaged predictions for each concentration.

rather than generalizing, which is known as overfitting. Therefore, we set the regularization constant to the value that minimizes the loss for the test set. Fig. 9 illustrates the optimized LASSO model predictions obtained by cross validation. For each concentration, the cross validation predictions were averaged and plotted along with the standard deviations. The predicted values vary linearly with the actuals. Figure 10

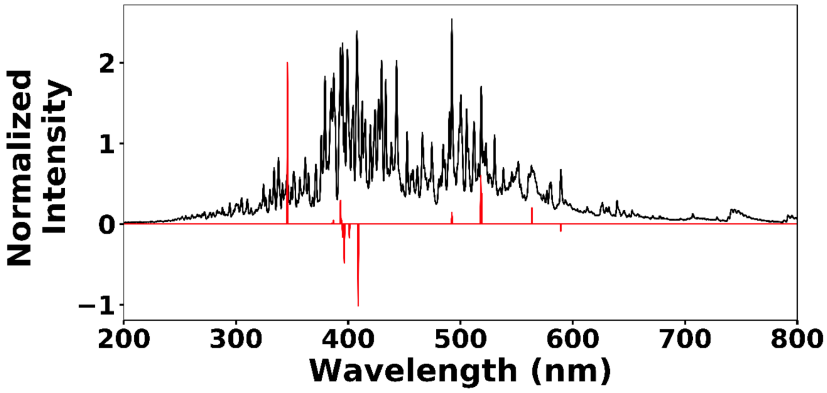

Figure 10: Ni 10ng spectrum (black line) and selected features by LASSO (red line).

shows the wavelengths chosen by LASSO and the mean spectrum for 10 ng. LASSO chose a few Ni emission peaks along with other features to build the model. The same optimization process was applied to other metallic elements specifically Cr, Cu, and Pb. Fig. 11 illustrates the resulting predictions and demonstrates the value of LASSO for predicting deposited mass from the spectra. To obtain the limit of detection (LOD),

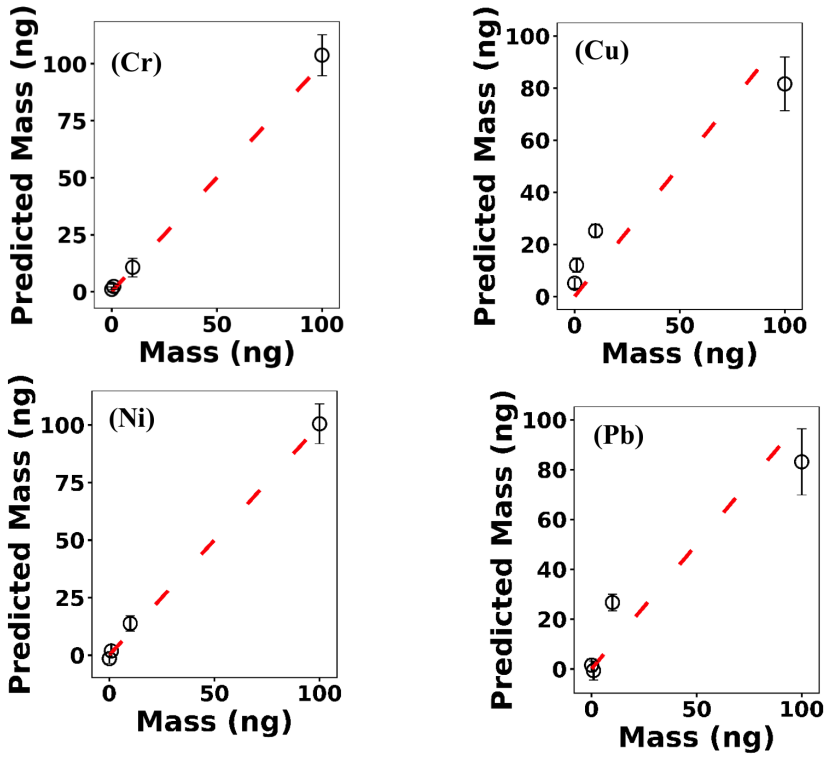

Figure 11: The optimized LASSO models predictions for Cr, Cu, Ni and Pb.

the following function of the LASSO coefficients θ_j was used:

$$LOD = 3\frac{\sigma_B}{S} = 3\sigma_B \|\boldsymbol{\theta}_B\| \tag{2}$$

where σ_B is the standard deviation of the background and $\|\boldsymbol{\theta}_B\|$is the Euclidean norm of LASSO coefficients. Table 3 reports the LODs of the studied metallic elements.

Multivariate regression models such as LASSO might be more powerful in detection and quantification

Table 3: Detection limits for various elements based on the LASSO and univariate models.

Element	LASSO	R^2	$\mathbf{MAE_{LASSO}}$	Univariate	R^2	$\mathbf{MAE_{Univariate}}$	Regularization cons.
Cr	3.55	0.99	6.71	3.28	0.98	3.83	0.0008
Cu	12.09	0.92	49.67	0.68	0.11	143.27	0.0006
Ni	9.60	0.98	6.67	2.32	0.88	68.63	0.0009
Pb	54.40	0.90	36.67	8.37	0.45	124.42	0.0018

over univariate models; however, there is no guarantee that multivariate models outperform simple linear regression Braga et al. (2010); Castro and Pereira-Filho (2016). To compare LASSO to univariate methods, we calculated the LODs using simple univariate linear regression based on the features selected by LASSO. Fig. 12 illustrates the LODs obtained using this univariate technique (circles) compared to LASSO LOD

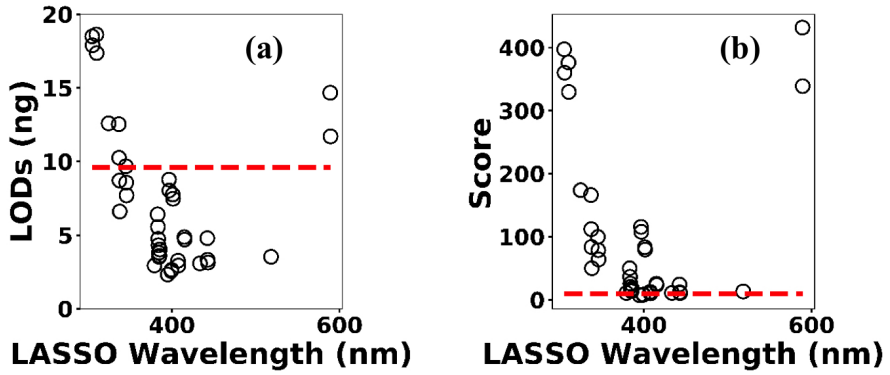

Figure 12: (a) the univariate LODs based on LASSO selected features and (b) LASSO and univariate models scores.

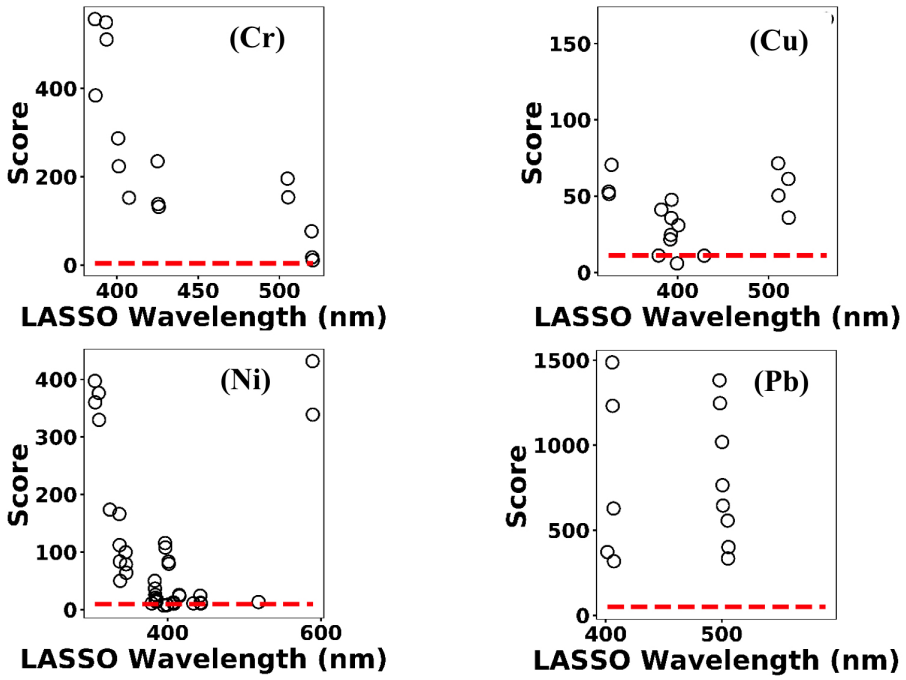

Figure 13: Model scores defined by equation 3 for Cr, Cu, Ni and Pb. Circles indicate univariate models scores and dashed lines correspond to LASSO scores.

(dashed line) for Ni. Considering only the sensitivity (LOD) is necessary but not sufficient for evaluating

model performance since low R^2 values are also problematic. Therefore, in order to incorporate both R^2 and LOD for model assessment, we defined a score as:

$$Score = (\frac{LOD}{R^2})^2 \tag{3}$$

Based on this definition, a model that has low LOD and high R^2 is desirable. LASSO score outperforms single feature linear regression for Pb, but the two methods were comparable for Cu, Ni, and Cr (Fig. 13). Other studies have reported that univariate techniques performed better than multivariate ones Braga et al. (2010); Castro and Pereira-Filho (2016). In LASSO, this may be related to the cost function defined for the regression (equation (1)). LASSO is a special case of elastic net family where both L1 and L2 norms are combined and used in the cost function. Considering the cost function in equation (1), the model goal is to minimize the prediction error and coefficient values (minimizing L1). This does not necessarily optimize LOD. Therefore, cost function minimization does not correspond to LOD minimization. Considering Fig. 12, using features defined by LASSO in a univariate model may yield better LOD than that obtained by LASSO alone. This might be an advantageous approach if the physical intuition of the features is not as important as detection of toxic metallic elements.

4 Conclusion

A cost-effective spark emission spectroscopy instrument was designed and developed to quantify toxic metallic elements targeted by US EPA and the California Air Resources Board. Costly components such as the spark generation system and delay generator were developed to lower the overall cost. An unsupervised learning technique was employed to detect outlier spectra. The cleaned spectra set was fed into LASSO for predicting the concentration of deposited samples on the ground electrode of the spark system from spectra obtained from the plasma. A combination of LASSO feature detection with univariate regression might improve the detection limits. Our results illustrate the promising realm of cost-effective sensors combined with advanced machine-learning techniques to provide data driven solutions to the traditional challenging problems.

Funding

California Air Resources Board (CARB).

Disclosures

The authors declare no conflicts of interest.

References

Abbasi, H., Rauter, G., Guzman, R., Cattin, P. C., and Zam, A.: Laser-induced breakdown spectroscopy as a potential tool for autocarbonization detection in laserosteotomy, Journal of biomedical optics, 23, 071 206, 2018.

Axente, E., Hermann, J., Socol, G., Mercadier, L., Beldjilali, S. A., Cirisan, M., Luculescu, C. R., Ristoscu, C., Mihailescu, I. N., and Craciun, V.: Accurate analysis of indium–zinc oxide thin films via laser-induced breakdown spectroscopy based on plasma modeling, Journal of Analytical Atomic Spectrometry, 29, 553–564, 2014.

Baudelet, M., Guyon, L., Yu, J., Wolf, J.-P., Amodeo, T., Fréjafon, E., and Laloi, P.: Femtosecond time-resolved laser-induced breakdown spectroscopy for detection and identification of bacteria: A comparison to the nanosecond regime, Journal of Applied Physics, 99, 084 701, 2006.

Braga, J. W. B., Trevizan, L. C., Nunes, L. C., Rufini, I. A., Santos Jr, D., and Krug, F. J.: Comparison of univariate and multivariate calibration for the determination of micronutrients in pellets of plant materials by laser induced breakdown spectrometry, Spectrochimica Acta Part B: Atomic Spectroscopy, 65, 66–74, 2010.

Brook, R. D., Franklin, B., Cascio, W., Hong, Y., Howard, G., Lipsett, M., Luepker, R., Mittleman, M., Samet, J., Smith Jr, S. C., et al.: Air pollution and cardiovascular disease: a statement for healthcare professionals from the Expert Panel on Population and Prevention Science of the American Heart Association, Circulation, 109, 2655–2671, 2004.

Buzea, C., Pacheco, I. I., and Robbie, K.: Nanomaterials and nanoparticles: sources and toxicity, Biointerphases, 2, MR17–MR71, 2007.

Castro, J. P. and Pereira-Filho, E. R.: Twelve different types of data normalization for the proposition of classification, univariate and multivariate regression models for the direct analyses of alloys by laser-induced breakdown spectroscopy (LIBS), Journal of Analytical Atomic Spectrometry, 31, 2005–2014, 2016.

Davari, S. A., Hu, S., and Mukherjee, D.: Calibration-free quantitative analysis of elemental ratios in intermetallic nanoalloys and nanocomposites using Laser Induced Breakdown Spectroscopy (LIBS), Talanta, 164, 330–340, 2017a.

Davari, S. A., Hu, S., Pamu, R., and Mukherjee, D.: Calibration-free quantitative analysis of thin-film oxide layers in semiconductors using laser induced breakdown spectroscopy (LIBS), Journal of Analytical Atomic Spectrometry, 32, 1378–1387, 2017b.

Davari, S. A., Masjedi, S., Ferdous, Z., and Mukherjee, D.: In-vitro analysis of early calcification in aortic valvular interstitial cells using Laser-Induced Breakdown Spectroscopy (LIBS), Journal of biophotonics, 11, e201600 288, 2018.

Davari, S. A., Taylor, P. A., Standley, R. W., and Mukherjee, D.: Detection of interstitial oxygen contents in Czochralski grown silicon crystals using internal calibration in laser-induced breakdown spectroscopy (LIBS), Talanta, 193, 192–198, 2019.

De Giacomo, A., De Bonis, A., Dell'Aglio, M., De Pascale, O., Gaudiuso, R., Orlando, S., Santagata, A., Senesi, G., Taccogna, F., and Teghil, R.: Laser ablation of graphite in water in a range of pressure from 1 to 146 atm using single and double pulse techniques for the production of carbon nanostructures, The Journal of Physical Chemistry C, 115, 5123–5130, 2011.

Diwakar, P., Kulkarni, P., and Birch, M. E.: New approach for near-real-time measurement of elemental composition of aerosol using laser-induced breakdown spectroscopy, Aerosol Science and Technology, 46, 316–332, 2012.

Diwakar, P. K. and Kulkarni, P.: Measurement of elemental concentration of aerosols using spark emission spectroscopy, Journal of analytical atomic spectrometry, 27, 1101–1109, 2012.

Do, H. and Carter, C.: Hydrocarbon fuel concentration measurement in reacting flows using short-gated emission spectra of laser induced plasma, Combustion and Flame, 160, 601–609, 2013.

Dyar, M., Carmosino, M., Breves, E., Ozanne, M., Clegg, S., and Wiens, R.: Comparison of partial least squares and lasso regression techniques as applied to laser-induced breakdown spectroscopy of geological samples, Spectrochimica Acta Part B: Atomic Spectroscopy, 70, 51–67, 2012.

Ferreira, E. C., Milori, D. M., Ferreira, E. J., Da Silva, R. M., and Martin-Neto, L.: Artificial neural network for Cu quantitative determination in soil using a portable laser induced breakdown spectroscopy system, Spectrochimica Acta Part B: Atomic Spectroscopy, 63, 1216–1220, 2008.

Fisher, B. T., Johnsen, H. A., Buckley, S. G., and Hahn, D. W.: Temporal gating for the optimization of laser-induced breakdown spectroscopy detection and analysis of toxic metals, Applied Spectroscopy, 55, 1312–1319, 2001.

Gent, J. F., Koutrakis, P., Belanger, K., Triche, E., Holford, T. R., Bracken, M. B., and Leaderer, B. P.: Symptoms and medication use in children with asthma and traffic-related sources of fine particle pollution, Environmental health perspectives, 117, 1168–1174, 2009.

Gottfried, J. L., De Lucia, F. C., Munson, C. A., and Miziolek, A. W.: Laser-induced breakdown spectroscopy for detection of explosives residues: a review of recent advances, challenges, and future prospects, Analytical and bioanalytical chemistry, 395, 283–300, 2009.

Hermann, J., Axente, E., Pelascini, F., and Craciun, V.: Analysis of Multi-elemental Thin Films via Calibration-Free Laser-Induced Breakdown Spectroscopy, Analytical chemistry, 91, 2544–2550, 2019.

Hu, S., Ribeiro, E. L., Davari, S. A., Tian, M., Mukherjee, D., and Khomami, B.: Hybrid nanocomposites of nanostructured Co 3 O 4 interfaced with reduced/nitrogen-doped graphene oxides for selective improvements in electrocatalytic and/or supercapacitive properties, Rsc Advances, 7, 33 166–33 176, 2017.

Hunter, A. J., Morency, J. R., Senior, C. L., Davis, S. J., and Fraser, M. E.: Continuous emissions monitoring using spark-induced breakdown spectroscopy, Journal of the Air & Waste Management Association, 50, 111–117, 2000.

Kiefer, J., Tröger, J. W., Li, Z., Seeger, T., Alden, M., and Leipertz, A.: Laser-induced breakdown flame thermometry, Combustion and flame, 159, 3576–3582, 2012.

Kotzagianni, M., Yuan, R., Mastorakos, E., and Couris, S.: Laser-induced breakdown spectroscopy measurements of mean mixture fraction in turbulent methane flames with a novel calibration scheme, Combustion and Flame, 167, 72–85, 2016.

Martin, M. Z., Labbé, N., André, N., Harris, R., Ebinger, M., Wullschleger, S. D., and Vass, A. A.: High resolution applications of laser-induced breakdown spectroscopy for environmental and forensic applications, Spectrochimica Acta Part B: Atomic Spectroscopy, 62, 1426–1432, 2007.

Matsumoto, A., Tamura, A., Honda, T., Hirota, T., Kobayashi, K., Katakura, S., Nishi, N., Amano, K.-i., Fukami, K., and Sakka, T.: Transfer of the species dissolved in a liquid into laser ablation plasma: an approach using emission spectroscopy, The Journal of Physical Chemistry C, 119, 26 506–26 511, 2015a.

Matsumoto, A., Tamura, A., Koda, R., Fukami, K., Ogata, Y. H., Nishi, N., Thornton, B., and Sakka, T.: On-site quantitative elemental analysis of metal ions in aqueous solutions by underwater laser-induced breakdown spectroscopy combined with electrodeposition under controlled potential, Analytical chemistry, 87, 1655–1661, 2015b.

Matsumoto, A., Tamura, A., Koda, R., Fukami, K., Ogata, Y. H., Nishi, N., Thornton, B., and Sakka, T.: A calibration-free approach for on-site multi-element analysis of metal ions in aqueous solutions by electrodeposition-assisted underwater laser-induced breakdown spectroscopy, Spectrochimica Acta Part B: Atomic Spectroscopy, 118, 45–55, 2016.

Mukherjee, D. and Cheng, M.-D.: Characterization of carbon-containing aerosolized drugs using laser-induced breakdown spectroscopy, Applied spectroscopy, 62, 554–562, 2008a.

Mukherjee, D. and Cheng, M.-D.: Quantitative analysis of carbonaceous aerosols using laser-induced breakdown spectroscopy: a study on mass loading induced plasma matrix effects, Journal of Analytical Atomic Spectrometry, 23, 119–128, 2008b.

Pope III, C. A., Burnett, R. T., Thun, M. J., Calle, E. E., Krewski, D., Ito, K., and Thurston, G. D.: Lung cancer, cardiopulmonary mortality, and long-term exposure to fine particulate air pollution, Jama, 287, 1132–1141, 2002.

Rovelli, S., Nischkauer, W., Cavallo, D. M., and Limbeck, A.: Multi-element analysis of size-segregated fine and ultrafine particulate via Laser Ablation-Inductively Coupled Plasma-Mass Spectrometry, Analytica chimica acta, 1043, 11–19, 2018.

Sacks, R. D. and Walters, J. P.: Short-time, spatially-resolved radiation processes in a high-voltage spark discharge, Analytical Chemistry, 42, 61–84, 1970.

Shepherd, J. E., Krok, J. C., and Lee, J. J.: Spark ignition energy measurements in Jet A, 2000.

St-Onge, L., Kwong, E., Sabsabi, M., and Vadas, E.: Quantitative analysis of pharmaceutical products by laser-induced breakdown spectroscopy, Spectrochimica Acta Part B: Atomic Spectroscopy, 57, 1131–1140, 2002.

Van Meel, K., Smekens, A., Behets, M., Kazandjian, P., and Van Grieken, R.: Determination of platinum, palladium, and rhodium in automotive catalysts using high-energy secondary target X-ray fluorescence spectrometry, Analytical chemistry, 79, 6383–6389, 2007.

Venecek, M. A., Zhao, Y., Mojica, J., McDade, C. E., Green, P. G., Kleeman, M. J., and Wexler, A. S.: Characterization of the 8-stage Rotating Drum Impactor under low concentration conditions, Journal of Aerosol Science, 100, 140–154, 2016.

Vincze, L., Somogyi, A., Osan, J., Vekemans, B., Török, S., Janssens, K., and Adams, F.: Quantitative trace element analysis of individual fly ash particles by means of X-ray microfluorescence, Analytical chemistry, 74, 1128–1135, 2002.

Walters, J.: Historical advances in spark emission spectroscopy, Applied spectroscopy, 23, 317–331, 1969.

Walters, J. P.: Spark discharge: Application multielement spectrochemical analysis, Science, 198, 787–797, 1977.

Yao, S., Xu, J., Zhang, L., Zhao, J., and Lu, Z.: Optimizing critical parameters for the directly measurement of particle flow with PF-SIBS, Scientific reports, 8, 1868, 2018.

Zanobetti, A., Franklin, M., Koutrakis, P., and Schwartz, J.: Fine particulate air pollution and its components in association with cause-specific emergency admissions, Environmental Health, 8, 58, 2009.

Zheng, L., Kulkarni, P., Zavvos, K., Liang, H., Birch, M. E., and Dionysiou, D. D.: Characterization of an aerosol microconcentrator for analysis using microscale optical spectroscopies, Journal of aerosol science, 104, 66–78, 2017.

Zheng, L., Kulkarni, P., and Diwakar, P.: Spatial and temporal dynamics of a pulsed spark microplasma used for aerosol analysis, Spectrochimica Acta Part B: Atomic Spectroscopy, 144, 55–62, 2018.